machines

MDPI

Article

Experimental Research on the Formation of the Third Body on the Friction Surface of Coal Cake Tamper Hammer Lifting Mechanism

Lin Huang, Shengfang Zhang, Bingtao Qin, Yu Liu and Zhihua Sha *

School of Mechanical Engineering, Dalian Jiaotong University, Dalian 116028, China; hlin1983@126.com (L.H.); zsf@djtu.edu.cn (S.Z.); qqq1262023@126.com (B.Q.); liuyu_ly12@126.com (Y.L.)
* Correspondence: zhsha_djtu@163.com

Abstract: A tamping machine is the key equipment of large coking coal cake forming in the steelmaking industry, where the loose coal is compacted into a coal cake by the reciprocating movement of its tamping hammer. In the long-term friction process, the third particle attached to the surface of the friction pair of the hammer lifting mechanism often causes the tamping hammer to slip and wear the tamping hammer friction plate, resulting in an insufficient height of the hammer, uneven work of the tamping hammer, coal cake collapse and other problems. In order to avoid the adverse effect of the third body on the surface of the friction pair, this paper studies the formation of the third body on the friction surface of the lifting hammer mechanism of the coal cake tamper. The cam material (Q345B) of the hammer lifting mechanism and the copper-based powder-metallurgy composite material of the friction plate of the tamping hammer are prepared into the pin-disk friction test disk and pin, respectively. Based on the characteristics of the friction temperature variation in the pin-disk test, an equivalent accumulation method is proposed, that is, the wear state of several samples at different wear times is equivalent to characterize the wear condition of a sample at different stages during continuous wear, and the different stages of the third body formation process are obtained. By analyzing the change of the composition of the third body and the content proportion of each element on the surface of the bottom plate at different wear times, it is determined that Cu is the key index of the third body. The content of the Cu element is used to characterize the content of the third body on the surface of the disk sample, and the formation rule of the third body on the surface of the disk is inferred. Through an image processing method of color analysis, the distribution law of the third body on the whole disk is identified. The properties of the third-body material on the disk surface are obtained by analyzing the changes of hardness and morphology at each friction stage. The results show that with the increase of friction time, the content of Cu on the disk surface increases to 22% and then decreases to 15%. The microhardness of the friction surface reaches its highest at 7 min, which is 1.4 times that of the Q345B material. The maximum disk surface roughness is 0.452 μm. Finally, the formation process of the third body is summarized in three stages: formation, equilibrium and damage. Therefore, the frictional properties of the surface of the friction pair vary from weak to strong to weak with the formation characteristics of the third body.

Keywords: hammer lifting mechanism; friction pair; pin-disk test; third body

Citation: Huang, L.; Zhang, S.; Qin, B.; Liu, Y.; Sha, Z. Experimental Research on the Formation of the Third Body on the Friction Surface of Coal Cake Tamper Hammer Lifting Mechanism. *Machines* **2023**, *11*, 660. https://doi.org/10.3390/machines11060660

Academic Editor: Sheng Li

Received: 20 May 2023
Revised: 14 June 2023
Accepted: 18 June 2023
Published: 19 June 2023

1. Introduction

With the continuous development of the machinery of the tamping coke oven in the direction of large scale and high efficiency, the coal cake tamping machine is the key equipment that restricts the quality of the tamping coke oven. The performance of the lifting mechanism directly determines the forming quality and stability of large-size coking coal cake, and then affects the quality of steel and iron making. Since the cam of the hammer lifting mechanism and the friction plate of the tamping hammer are extrusion friction, as

shown in Figure 1, the appearance of the third body on the surface of the friction pair will cause the mechanical properties of the friction surface to change, resulting in the sliding of the cam and the friction plate, resulting in insufficient lifting height of the tamping hammer, uneven work of the tamping hammer, and finally the collapse of the coal cake. Therefore, in this paper, the third-body formation rule of the material friction and wear of the cam and tamping hammer friction plate is studied.

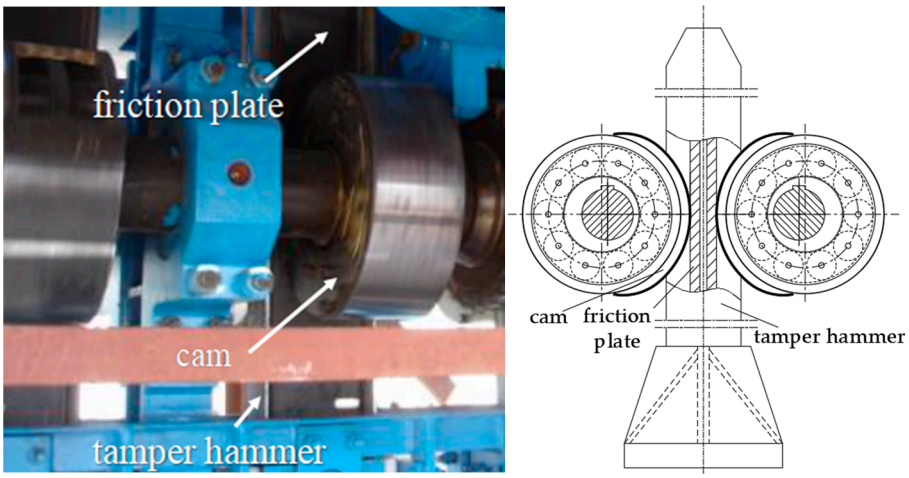

(**a**) Physical picture (**b**) Structure sketch

Figure 1. Tamper hammer lifting mechanism friction surface.

In recent years, most of the studies on the surface topography of friction pairs have adopted a fractal function to simulate the roughness surface and further study the change of the contact properties of friction surfaces. Li et al. [1] found that the surface of the rough slider generated by a fractal function was closer to the real surface topography for studying the real contact area, contact pressure, contact stress and deformation. Lu et al. [2] generated and analyzed artificial fractal curves by combining the W-M function with traditional parameters, which could also be used to analyze the influence of the texture distribution on other pavement performance. Wang et al. [3] proposed a fretting damage model based on fractal theory; the rough contact surface was represented by the Weierstrass–Mandelbrot function of fractal theory, and they established a corresponding contact parameter analysis method. Qiang et al. [4] proposed an Iterative method for calculating the time-varying wear of rough fractal surfaces, analyzed the contact mode between the microconvex peak and the rigid plane and established the relationship between the wear deformation and the real contact area. Zuo et al. [5] presented a new methodology of wear state recognition by using fractal parameters, multifractal parameters and recurrence parameters. The wear states could be identified effectively by the relationship between nonlinear state points and the steady-state sphere. Xu et al. [6] established a characterization framework for inspecting worn surface topography variations under a sliding-rolling contact, by combining a 3D surface reconstruction and the computed fractal dimension.

As for the study of the third body on the friction and wear surface, a large number of scholars have mainly focused on the microstructure law and the change law of the third body on the mechanical properties of the friction surface. Since Godet [7] first defined the concept of frictional third-body theory in 1984, scholars have continued to deepen their research on the third body. Berthier et al. [8] analyzed fretting wear and fretting fatigue and found they were governed by the rate of formation of third-body materials between the initial contact surfaces. Eriksson et al. [9] considered that the discontinuous distribution of the friction layer was not necessarily caused by the convex deformation of the surface. Xu et al. [10] uncovered that the factors could make the debris layer or third body remain on the contact surfaces and would decrease the friction coefficient and fretting wear. Mou et al. [11] considered that the morphology of the third-body layer would be dif-

ferent with the change of friction conditions. Dolgopolov et al. [12] invested the structural features of the third body appearing, with the help of mineral friction modifiers. Yang [13] found that the composition of the third-body layer contained brake disc material and brake pad material debris and the oxide of the friction pair material. Bulnes [14] researched the mechanochemical friction of the third body and found that the mechanochemical formula for the 3D body's boundary friction fell within the scope of the physics of chaos and the phenomena of auto-organization of surfaces. Perumean [15] derived the equations required to predict the forces on the free-body diagrams of two sliding bodies when observed from a third moving body. Lei et al. [16] studied microstructural changes of C/C composites after the braking test and established a microstructural model of the worn surface layer. N. Diomidis et al. [17] researched the change of friction coefficient and the influence of the microstructure and chemical composition of the third object with the change of critical contact pressure. Stoyanov et al. [18] analyzed that experimental and numerical atomistic investigation of the third-body formation process in dry tungsten/tungsten carbide tribological couples. Lepesant et al. [19] assessed the third-body particles circulation in a high temperature friction contact. Su et al. [20] investigated the tribological properties of copper-based friction materials with an exogenous copper powder third body and the friction coefficient could be increased on average by 0.03 in the presence of exogenous copper powder on the friction surface compared with nonexogenous copper-based friction materials. Gao et al. [21] proposed a mechanically assembled method which compacted several component sheets in order to further increase the understanding of the evolution of each component and the corresponding third body in the friction process. Zun et al. [22] proposed a physically based relationship between the debris expulsion's limited wear rate and the contact size, and the relationship was able to account for differences in wear rates observed in tests conducted with different contact geometries over a range of durations. Liskiewicz et al. [23] combined surface morphology with the progressive process of interfacial oxidation and observed a strong relationship between surface roughness and electrical contact resistance. Zhang et al. [24] conducted a pin-disk test at 400–800 °C, and the results showed that the friction film changed from a single-layer structure to a double-layer structure with increasing temperature, and the wear mechanism changed from abrasive wear on the surface of the friction disc to adhesive wear on the friction film. Mondal [25] analyzed the wear performance of this newly developed steel and concluded that the work hardening as well as improved yield strength of the HSLA steel led to the superior wear performance. Hu [26] observed that dislocation plasticity induced two failure patterns of the third-body wear by molecular dynamics simulations. Ahmadi et al. [27] studied the third-body effects on the fretting wear of Hertzian contacts in the partial slip regime via a finite element model. Shpenev et al. [28] analyzed the influence of the presence of a third-body film and estimated its thickness on the coefficient of friction and the intensity of material wear. Yulong et al. [29] utilized bearing steel (100Cr6) pins and discs in a flat-on-flat contact in experiments together with 5 and 13 m Al_2O_3-based slurries as interfacial media to shed light on the acting mechanisms. Brink et al. [30] found that that transition was controlled by the growth and increasing disorganization of the particles with the increasing sliding distance.

A lot of research was conducted on the surface topography analysis of friction pairs, the microstructure of the third body on the friction and wear surface and the change of the mechanical properties of the third body on the friction surface. At the same time, it also showed that the influence of the third body at the friction interface on the mechanical properties of the friction surface was also different with the different friction conditions, friction materials and use conditions. Few people studied the changes of the third body on the surface of friction pairs from the perspective of the formation process of the third body. In order to avoid the adverse effect of the third body on the surface of the friction pair of the hammer mechanism of the tamping machine, the third-body formation rule of the material friction and wear of the cam and the friction plate of the tamping hammer is studied experimentally in this paper.

The samples of pin and disk are made with the same material as the friction plate and cam of the tamping hammer. Based on the analysis of the Cu content, surface hardness and roughness, the formation process, composition and morphological characteristics of the third body on the surface of the friction pair are studied, and the frictional properties of the surface of the friction pair are summarized. It provides a reference for understanding the formation law of the third body on the friction pair surface of the lifting mechanism in the tamping process. The main innovation of this paper can be summarized as follows:

- An equivalent accumulation method is proposed to use the wear states of several samples under different wear times to equivalently characterize the wear conditions of a sample in different stages of continuous wear, and the different stages of the third-body formation process are obtained.
- By analyzing the microscopic changes in the composition of the third body at different wear times and the content proportion of each element on the surface of the disc, it is determined that Cu is the key indicator of the emergence of the third body. The content of the Cu element is used to characterize the content of the third body on the surface of the disk sample, and the formation rule of the third body on the surface of the disk is inferred.
- Through an image processing method of color analysis, the distribution law of the third body on the whole disk is identified. The friction performance of the disk surface is obtained by analyzing the changes of hardness and morphology at each friction stage.

The rest of this paper is organized as follows. In Section 2, the experimental design of the third-body formation process and the proposed method are introduced. The third body's analysis with different friction times is introduced in Section 3. Performance tests of the friction surface at different friction times are presented in Section 4**.** Finally, Section 5 concludes the paper.

2. Experimental Design of the Third-Body Formation Process

2.1. Test Method

The friction pair of the lifting hammer mechanism changes the speed and temperature of the cam material constantly during the friction process. However, from a specific moment in the lifting hammer mechanism process, the friction can be regarded as constant velocity friction, and from the whole service cycle of the lifting hammer mechanism's friction pair, the formation of the third-body surface is a result of long-term accumulation, and the constant velocity test is beneficial to shorten the test cycle.

During the lifting process of the tamper, the cam friction plates on both sides of the tamper hammer make the hammer lift. In the friction test, the contact form of the pin-disk friction pair is consistent with the form of the friction pair of the hammer mechanism, so the two materials of the friction pair were made into pin-disk friction samples for testing on an MMW-1A friction and wear test machine shown in Figure 2. The cam material of the disk sample was Q345B, which is commonly used for the friction pair of the hammer mechanism at present, and its size was Φ54 mm × 10 mm. The pin sample was a copper-based powder metallurgy composite material based on tin bronze, and its size was Φ4.8 mm × 12.7 mm. The sample is shown in Figure 3.

2.2. Test Plan

In order to ensure that the friction surface did not produce serious abrasions and the copper-based powder-metallurgy composite did not collapse, the parameters selected for the test were a 60 N friction pressure and 1200 r/min friction rotation speed. A continuous third body could be generated on the surface of the disk sample after 10 min of the test.

Therefore, in order to observe the different stages of the formation process of the third body, ten identical disk samples were numbered 1–10, and each number corresponded to the friction time of the disk sample. The friction speed of 1200 r/min and the friction pressure of 60 N were selected for the test.

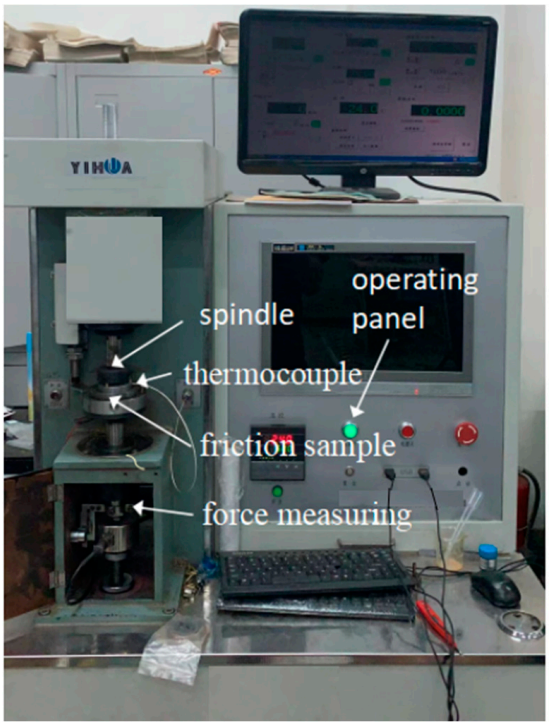

Figure 2. MMW-1A microcomputer-controlled friction and wear tester.

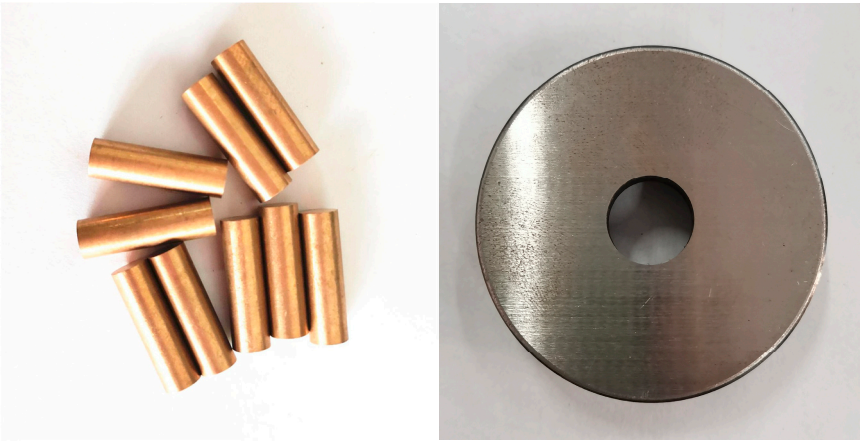

(**a**) Pin samples (**b**) Disk sample

Figure 3. Pin-disc sample.

In the test, a PT100 thermocouple was used to record the temperature changes on the surface of the disk samples in 10 groups of tests. During the test, the thermocouple was used to monitor the temperature change of the friction surface in real time, and then, the morphological characteristics of the third body were analyzed by a ZWSP-2KCH optical microscope. On the premise that the test rotation speed, test pressure and sample material were consistent, different test times were selected. If the temperature change trend of the disk sample surface of the 10 groups was similar, it meant that the 10 groups of tests could be regarded as different moments in the process of the formation of the third body.

Figure 4 shows the temperature change curves of 10 samples at different friction times. According to the Figure 4, the temperature variation trend of the 10 samples during the test was similar. When the test time was less than 4 min, the temperature change on the surface of the samples was in a rapid rise stage, the temperature increase rate was roughly the same, and the absolute temperature difference was about 15 °C. When the test time was

more than 4 min, because the heat dissipation rate of the sample increased, the temperature increase speed slowed down, showing a gradually stable state, and at that time, the absolute temperature difference was about 5 °C. When analyzing the formation process of the third body, the 10 sets of tests could be defined as different stages of the same friction process.

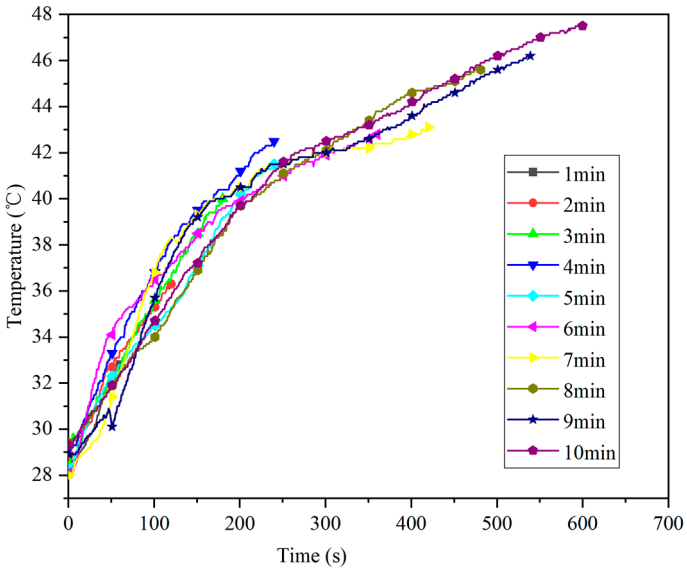

Figure 4. Temperature change curves of samples at different friction times.

3. Third-Body Analysis with Different Friction Times

3.1. Third-Body Surface Composition Analysis

After the test, an EDS analysis using a JSM6360-LV scanning electron microscope was performed on different positions of the friction surface of the sample after the 7 min friction test, as shown in Figure 5. As can be seen from the energy spectrum analysis results outside the adhesion pit in Figure 5a, there was a large amount of Cu element on the friction surface, indicating that there was a large quantity of friction plate material components. As can be seen from the energy spectrum analysis results of the compaction region in Figure 5b, the contents of Fe and Cu on the friction surface were both relatively high and the values were close to each other, indicating that the pin material was well combined with the disk material. The analysis results of the elements on the surface of the disk after the test showed that the distribution of the Cu element on the friction surface was significant, but by comparing the chemical composition of the disk material Q345B in Table 1, it can be seen that there was no Cu element in the disk material. Therefore, the Cu element can be used as the key indicator to judge whether there is a third body, and the location with a higher Cu content can be considered as the location where the third body is distributed.

Table 1. Chemical composition of Q345B.

Element	C	Mn	Si	P	S	Cr	V	Nb	Ti
Content (%)	0.2	1.7	0.5	0.035	0.035	0.3	0.15	0.07	0.2

An EDS analysis was conducted on the surface of 10 samples after the test, and the results are shown in Table 2. According to the results, with the increase of friction time, the content of the Cu element on the friction surface increased continuously. When the friction time was 7 min, the content of the Cu element reached 22 wt%, and with the increase of friction time, the content of the Cu element decreased.

Table 2. Cu content of the third body on surfaces at different friction times.

Friction Time (min)	1	2	3	4	5	6	7	8	9	10
Cu content (wt%)	0.74	1.28	3.2	5.4	8.67	17.5	22	18.4	13.7	15.3

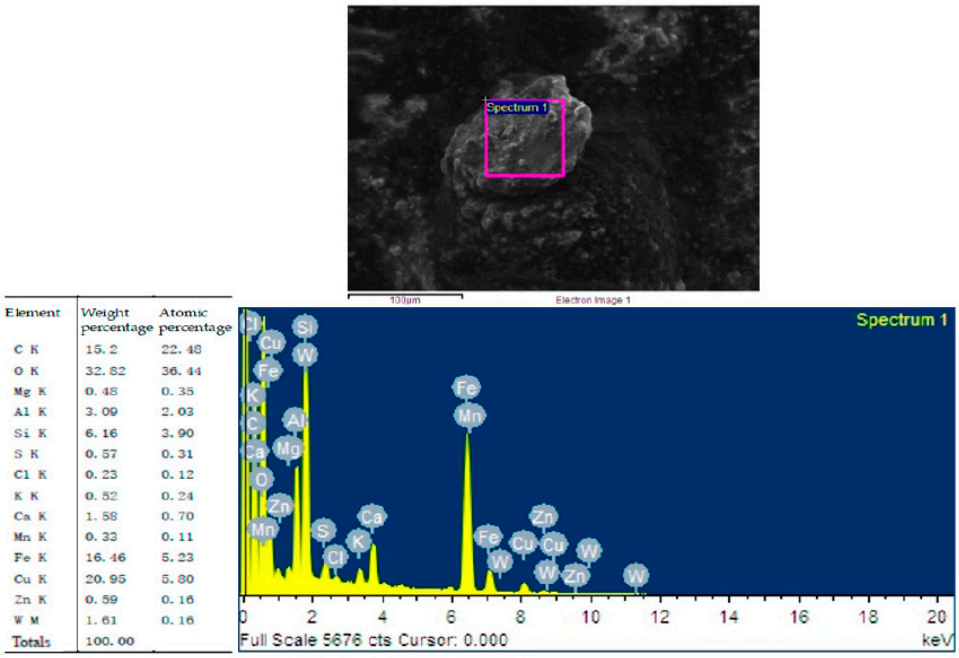

(**a**) Results of the energy spectrum analysis outside the adhesion pit

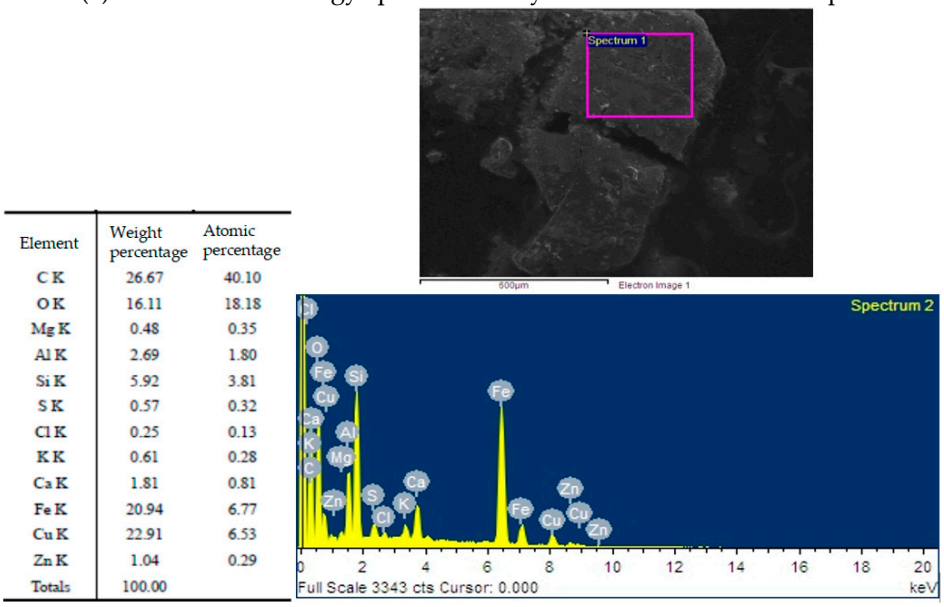

(**b**) Results of the energy spectrum analysis in the compaction region

Figure 5. Energy spectrum analysis at different positions on the surface of the sample with a friction time of 7 min.

Therefore, according to the results of the energy spectrum analysis, the third body of a small area was generated on the friction surface within 1 to 3 min, but the content of the Cu element was insufficient, the components transferred from the copper-based powder-metallurgy materials of the pin were fewer, and the complete and compact third

body could not be formed. With the continuous friction process, the compaction region produced the third body, and the Cu content increased continuously. The mass percentage of the Cu element showed a stable state, and the content of the third-body component had no obvious change from 4 to 7 min. During 8–10 min, the content of the Cu element decreased compared with that of the previous period. It can be seen from the analysis that the third body in the compaction region was destroyed by friction, but the Cu content remained at 15 wt%, which indicated that the damage degree of the continuous friction process to the third body in the compaction region was limited.

3.2. The Third-Body Particle Analysis

The shape and size of the grinding chips produced in the friction process showed different characteristics. The state and wear degree of the friction system can be monitored and judged with the aid of dust sampling. If the friction material is slightly worn, it forms a fine, smooth surface grinding chip, the size is generally about 0.01~2 μm; if the friction material is severely worn, the size of the grinding chips is in the range of 20 to 200 μm [31]. In the process of producing the third body, one of the samples in the three stages (the friction time varied was 2 min, 5 min and 8 min, respectively) was selected, and the wear chips generated during the test are collected, as shown in Figure 6. It can be seen that when the friction time was 2 min, the size of the friction chips generated was generally less than 10 μm, and the friction material was slightly worn. When the friction time was 5 min, the chip size increased to about 30 μm; when the test time was 8 min, the maximum size of the debris was about 100 μm. It can be seen from the figure that there were two forms of grinding chips: spherical and lamellar.

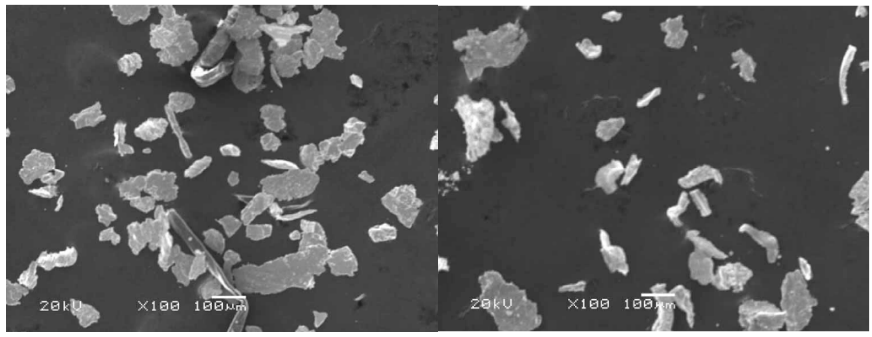

(**a**) 2 min (**b**) 5 min

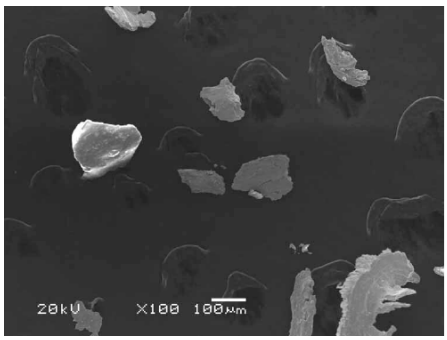

(**c**) 8 min

Figure 6. The micromorphology of abrasive chips at different time.

This is because a spherical grinding chip is formed by the mechanical mixing of the friction pair's transfer material as the third-body particle participating in the friction process. The lamellar chip is formed because the microconvex body is cut by the friction surface, and the friction surface cracks. The large area of contact between the chip and the friction surface is an important reason for the formation of the third body on the surface.

3.3. Analysis of Surface Morphology during the Formation of the Third Body

The surface morphology of the third body of 10 samples was observed by a ZWSP-2KCH optical microscope, and the change laws of the third body were analyzed. Figure 7 shows the surface topography comparison of 10 samples at a magnification of 200 times, with surface machining traces in the longitudinal direction and friction traces in the transverse direction. It can be seen in Figure 7 that at the beginning of friction, there were obvious longitudinal machining traces on the surface of the sample. With the increase of friction time, the longitudinal machining traces were gradually covered by the third body formed on the sample's surface. When the friction time increased to 10 min, a continuous third body was formed on the sample's surface.

At the initial stage of the friction test, when the friction time was 1 min, furrows of different depths appeared on the surface of the sample, as shown in Figure 7b. As the test proceeded, when the normal load exceeded the material yield limit, the mesh degree of the friction component or microconvex body with a high hardness of copper-based powder-metallurgy materials was enhanced, and the microcutting effect of the hard particles could cause the furrow type destruction of the sample surface of the disk material. At the same time, it could be observed that the bulk discrete third body began to appear on the surface of the friction sample, as shown in Figure 7c. As the friction time increased, the area of the bulk third body on the friction surface increased, and the friction surface was rough, as shown in Figure 7d. That stage could be regarded as the formation stage of the third body. In that stage, the friction surface temperature was low, and the main form of wear was abrasive wear. Under the abrasive wear mechanism, a large amount of abrasive debris with the same composition as the friction pair material would form on the friction surface.

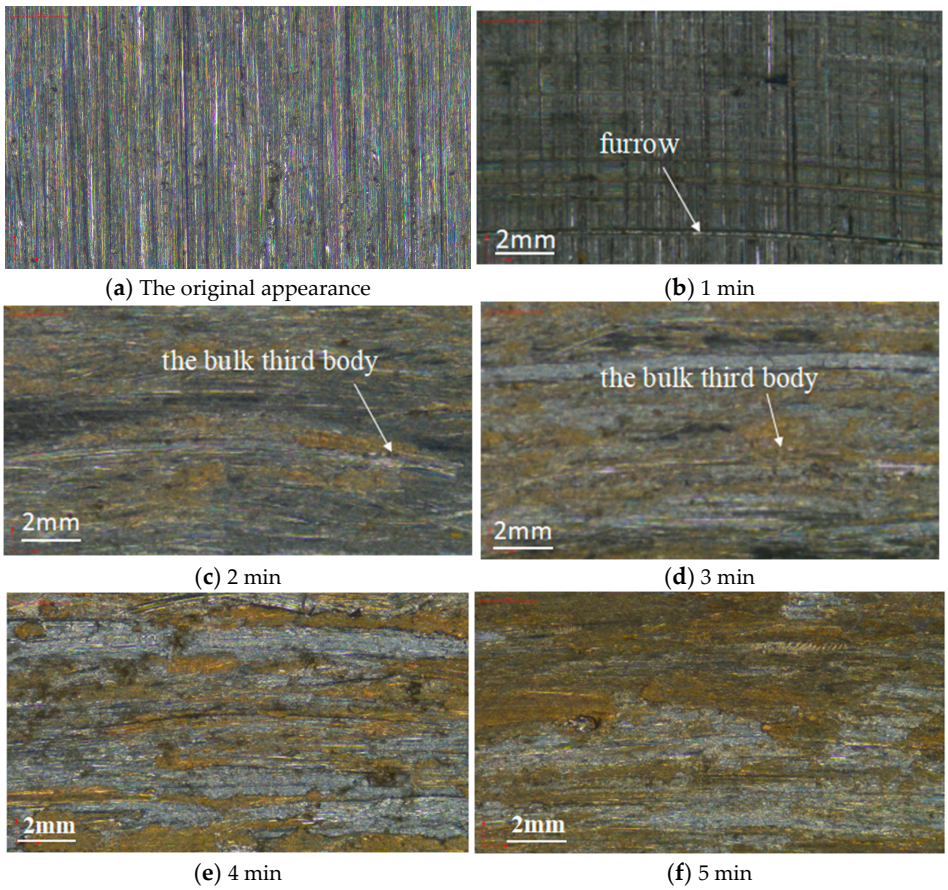

(**a**) The original appearance (**b**) 1 min

(**c**) 2 min (**d**) 3 min

(**e**) 4 min (**f**) 5 min

Figure 7. *Cont.*

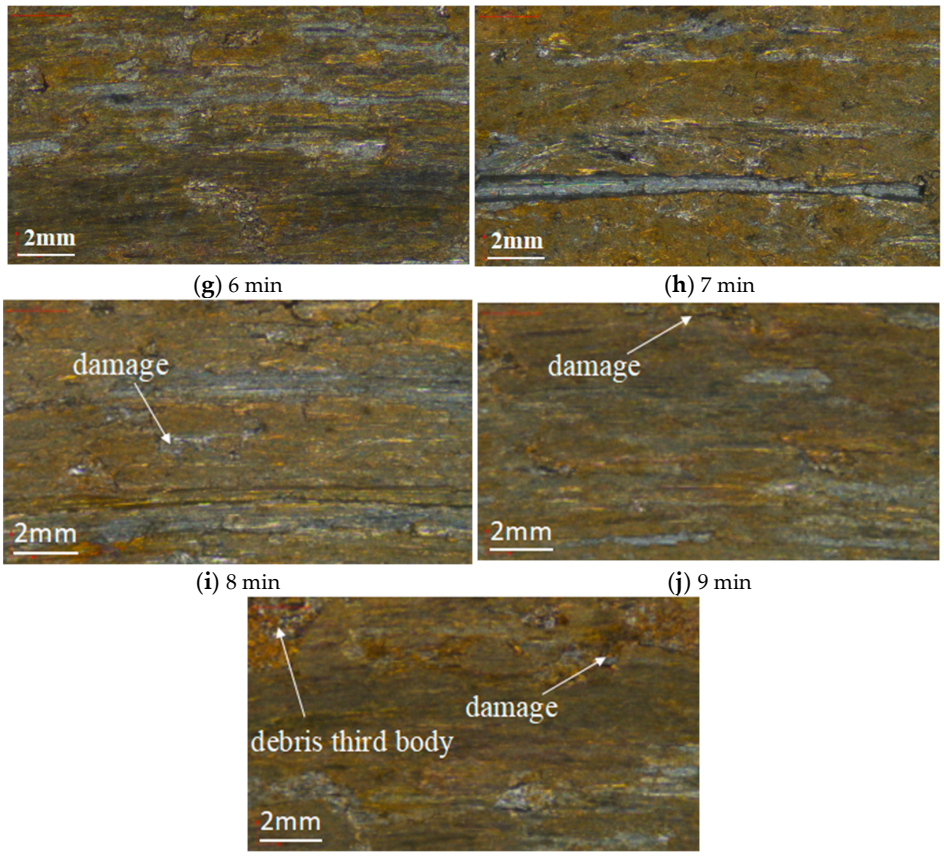

(**g**) 6 min (**h**) 7 min

(**i**) 8 min (**j**) 9 min

(**k**) 10 min

Figure 7. The surface morphology of the samples at different friction times.

With the extension of the friction time, it could be observed that the area of the third body on the friction surface increased, the original bulk third body was converted to a continuous third body, and the third body gradually covered the surface of the disk sample, as shown in Figure 7e–g. This is because during the friction process, the abrasive debris gradually increases and piles up in the furrow position. When it accumulates to a certain extent, the welding effect occurs between the debris of the third body under the action of compressive stress. At that time, the parts of the third body with a large local thickness expand and thus form the continuous third body. When the friction time was 7 min, the temperature of the friction surface rose, causing a plastic deformation of the local material, and the third body grew stably. The thickness of the third-body layer on the friction surface increased, and its density also began to increase, as shown in Figure 7h. At that time, the formation speed and destruction speed of the third-body layer reached a state of equilibrium, and the third-body particle formed in the initial stage of friction bore repeated grinding on the friction surface. In that stage, the third-body layer was in a dynamic equilibrium stage of alternating formation and destruction.

As the friction continued, it could be observed that the area of the third body on the friction surface decreased to a certain extent. At that time, the formation of the third body on the friction surface reached a maximum, and the third-body layer began to be damaged. Damage such as material peeling could be observed on the friction surface, as shown in Figure 7i,j. At the same time, a small amount of new third-body debris could be found in the damage, as shown in Figure 7k.

During the initial friction, the copper particles spread evenly on the surface of the disk. With the friction progress, the third-body protective layer formed by the compacted copper particles gradually fell off, each peel was lumpy, and the lumpy compacted copper particles aggravated the surface wear, resulting in the phenomenon of damage on the disk surface.

In order to calculate the percentage of copper element on the surface of the disk sample, Photoshop image analysis software was used to analyze the color of the surface of the disk sample. The percentage of the third-body area was obtained by Formula (1).

$$\frac{\text{testing area (At)}}{\text{reference area (Ar)}} = \frac{\text{display pixels of testing area (Pt)}}{\text{display pixels of reference area (Pr)}} \quad (1)$$

The percentage growth rate of the third body was the difference between the area of the third body at time t and the area of the third body at time t-1 divided by the reference area, where t is the friction time.

The extraction and analysis of the elements of the macromorphology image of the sample surface in Figure 7 uncovered the percentage of the third-body area in the disk area at different friction times shown in Figure 8. A small amount of the third body appeared in 1 min. From 2 min to 10 min, the percentage of the third body area in the disk area increased from 26.48% to 94.19% as shown in Table 3. From 1 min to 10 min, the percentage growth rate of the third body increased first and then decreased, reaching 24.18% at 2 min.

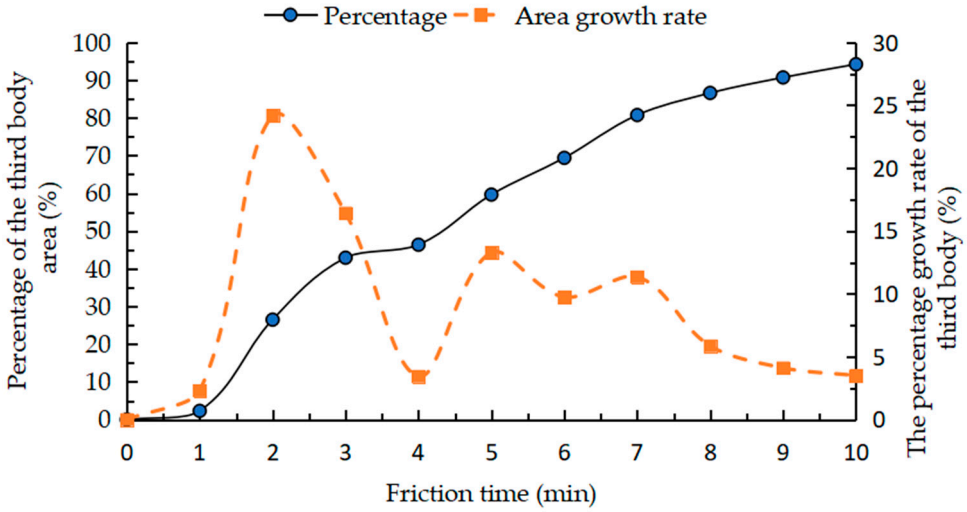

Figure 8. The percentage of the third body at different friction times.

Table 3. Percentage of the third body at different friction times.

Friction Time (min)	1	2	3	4	5	6	7	8	9	10
Percentage (%)	2.3	26.48	42.9	46.34	59.63	69.37	80.7	86.6	90.69	94.19
The percentage growth rate of the third body (%)	2.3	24.18	16.42	3.44	13.29	9.74	11.35	5.86	4.11	3.5

This is because at the beginning of the surface of the friction sample, the discrete third body is adsorbed on the sample's surface. With the gradual increase of the third body, the massive third body forms a continuous third body and is still adsorbed on the sample's surface. As the friction time continues to increase, the third layer alternates between formation and destruction, and finally, some parts fall off, so the growth rate decreases accordingly.

4. Performance Test of the Friction Surface at Different Friction Times

4.1. Microhardness Analysis

The microhardness was measured by an HV1000Z micro-Vickers hardness tester, according to ISO 6507-1, the selected test force was 200 g and a load-holding time of 10 s.

Three points were measured on the sample's surface, and the average value was taken as the final result. The results in Figure 9 show that the microhardness of the friction surface continued to increase with the extension of the friction time. When the friction time was 7 min, the disk surface hardness reached the highest value of 457HV1/10, about 1.4 times that of the Q345B material. When the friction time was longer than 7 min, the microhardness of the friction surface decreased slightly. After the third body was formed on the friction surface, the microhardness of the material was greater than that of the matrix metal.

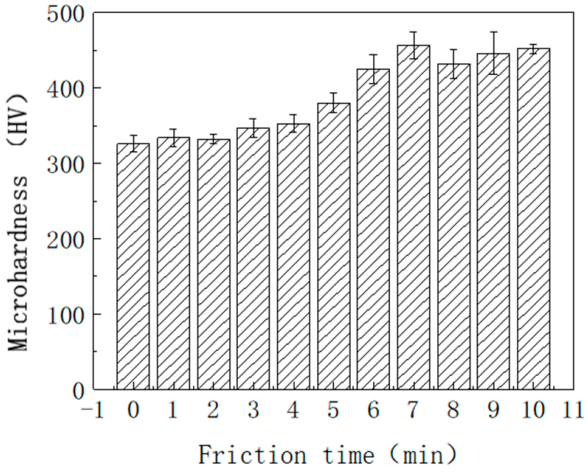

Figure 9. Microhardness of the friction surface at different friction times.

The reason was that the third body formed on the surface of the friction material was composed of a large number of metal compounds, and the crystalline fibrosis due to the extrusion of abrasive chips during friction resulted in the hardness of the microbonded debris in the process of friction to also be large. It also showed that the copper particles on the surface of the disk were first compacted and then fell off into chunks.

4.2. Surface Roughness Analysis

The surface roughness of the samples was measured by an IFM-G5 three-dimensional-topography-measuring instrument, the sampling length was selected as 2.5 mm, and the evaluated length was 5 times the sampling length. The 3D surface topography of the samples at different friction times is shown in Figure 10. The average value of Ra at different positions in the same region of samples of different disks under different wear times was measured. The measurement results are shown in Figure 11. The results showed that when the friction time was less than 3 min, the friction surface's roughness value increased with the friction time increase, and the maximum value of Ra was 0.452 μm. When the friction time was greater than 3 min, the roughness value of the disk surface started to decrease. When the friction time was 7 min, the friction surface was the smoothest, and the Ra value was 0.201μm, indicating that the quality of the third-body layer was good at that time. When the friction time was longer than 7 min, the surface roughness began to increase slightly, indicating that the third-body layer began to be damaged at that time. According to the analysis of Figure 11, the roughness of the third-body layer was smaller than that of the matrix.

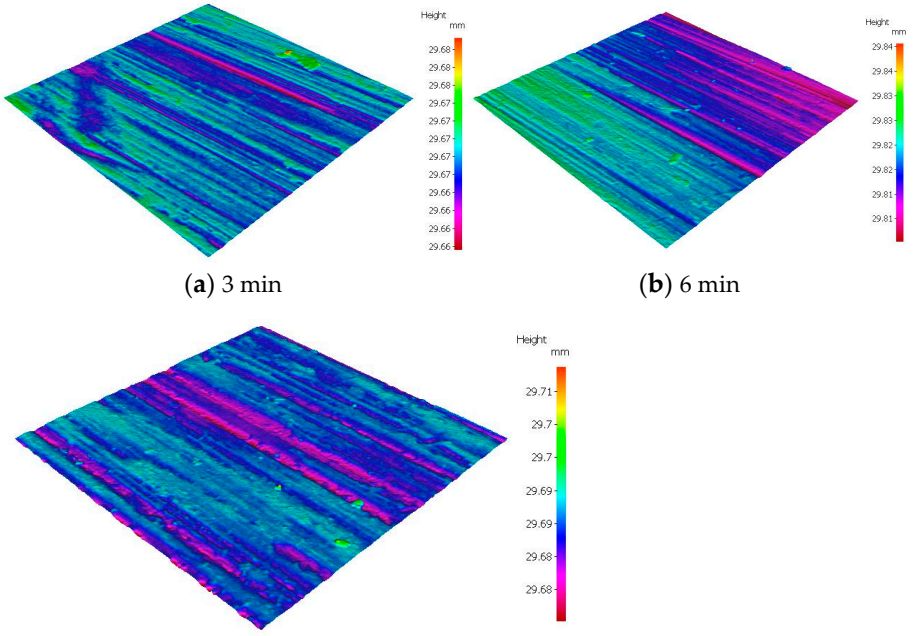

(**a**) 3 min (**b**) 6 min

(**c**) 9 min

Figure 10. Three-dimensional surface topography of the samples at different friction times.

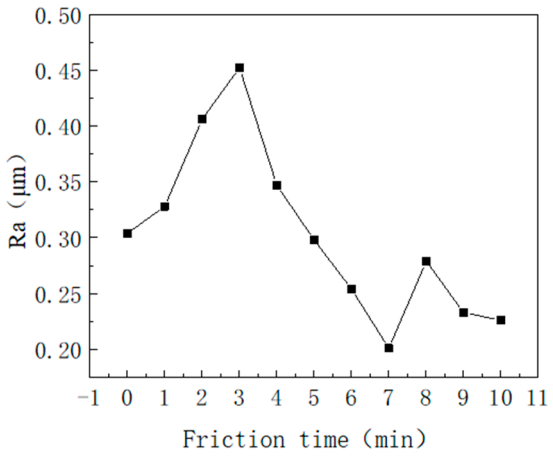

Figure 11. Roughness of the friction surface at different friction times.

This is because with the progress of the friction process, friction components with a low hardness or microconvex bodies with a low hardness on the friction surface of copper-based powder-metallurgy materials fill the furrows and wear marks on the surface of disk material samples, and a continuous and bright third body is formed on the surface of disk samples, which reduces the grinding effect of grinding chips on the worn surface morphology. The results showed that the copper particles had the effect of filling the surface gullies and improving the roughness, but the surface roughness also fluctuated with the falling off of the compacted copper particles, which affected the friction stability.

Through the composition analysis of the third body surface, the surface morphology analysis during the formation of the third body and the surface roughness analysis, it can be seen that under the friction conditions of the pin-disk material, a continuous and bright third body was produced on the friction surface. The microhardness and surface roughness of the friction surface at different times were different, so the influence on the friction behavior was also different. The formation of the third layer on the friction surface was a dynamic process that could be divided into three stages:

(1) Formation stage (1–3 min): At the initial friction stage between 1 min and 3 min, the friction surface directly contacted, and the microconvex body on the friction surface engaged. With the relative motion of the friction pair, the microconvex body was welded under the influence of temperature and normal force. Once the welding strength exceeded the shear strength of the material, the microconvex body was stripped from the friction surface, resulting in grinding chips. At the same time, the friction surface was affected by the cutting of the microconvex body, forming furrows of different depths. These furrows cut the friction material into grinding chips, which accumulated in large quantities at the front of the microconvex body and became a discrete third body under the action of the normal force. The third body formed at this stage had poor friction and wear performance, a discontinuous distribution on the friction surface, a small hardness and a large roughness, which made it difficult to provide effective protection for the friction surface. The form of wear was abrasive wear and adhesive wear of the pin material.

(2) Equilibrium stage (4–7 min): As the friction continued, the accumulated debris formed a continuous third body. Under the condition of high-speed friction, with the increase of time, the heat was released during the friction process, which accelerated the oxidation reaction of the microconvex body on the friction surface and formed a dense oxide film on the friction surface. With the further progress of friction, the oxide film was destroyed by adhesive wear, resulting in oxide grinding chips. Oxide grinding chips, disk-material grinding chips and pin-material grinding chips were mixed to form the third body. Under the influence of a normal load, these mixtures covered the friction surface to form a dense film layer, which effectively protected the friction surface. At that stage, oxidation wear and abrasive wear were the main wear forms.

(3) Damage stage (8–10 min): The third-body layer was formed. Due to the combined action of friction pressure and shear force, the third-body layer was damaged and material stripping began to occur. Part of the friction surface was exposed and scratched by the free third body. In the damage stage, fatigue wear and abrasive wear were the main wear forms.

5. Conclusions

In this paper, based on a friction and wear test of pin-disk material made of a cam and tamping hammer friction plate, an equivalent accumulation method was proposed according to the characteristics of friction temperature. According to this method, the different stages of the formation of the third body on the disk surface were obtained. According to scanning electron microscopy, electron optical microscopy and an energy spectrum analysis, copper was determined to be an important index of the third-body observation. The formation rule of the third body on the surface of the disk was deduced. The distribution of the third body on the whole disk was discussed by using an image processing method of color analysis. The friction properties of the disk surface were obtained by observing the changes in the hardness and morphology of the third-body material at each friction stage. The conclusions are as follows:

(1) In the process of friction, the surface of the cam generates a yellow continuous third-body layer; this third-body layer contains the transfer component of the friction plate material; Cu element can be used as the evaluation basis for the formation of the third body on the cam surface.

(2) The formation process of the third body of the cam material can be divided into three stages, namely, the formation stage, the dynamic equilibrium stage and the damage stage. The formation process of the third body is accompanied by oxidation wear and fatigue wear, and the formation and failure process of the third body appear alternately.

(3) The third-body material on the friction surface of the lifting hammer mechanism is a metal compound composed of the cam material, the tamping hammer friction plate material and the corresponding oxide. During the formation of the third-body layer, the microhardness of the sample surface increases compared with the matrix material, and the maximum can reach 1.4 times that of the cam material.

6. Prospect of Research Work

By testing the surface characteristics and performance of the third body, the particle adhesion state on the disk's surface during the formation of the third body was obtained.

In future work, we will further test on the actual equipment in a field environment to study the influence of more factors on the third body of the friction pair of the hammer lifting mechanism.

Author Contributions: L.H. and Z.S. conceived the idea of this work; L.H. and S.Z. conducted the experiment; data curation, B.Q.; original draft preparation, L.H.; review and editing, Z.S. and Y.L. All authors have read and agreed to the published version of the manuscript.

Funding: This research was funded by the National Natural Science Foundation of China (no. 51675075), Scientific Research Project of the Education Department of Liaoning Province (no. LJKZ0479), and Dalian Science and Technology Innovation Fund (no. 2021JJ12GX009).

Data Availability Statement: The data used to support the findings of this study are available from the corresponding author upon request.

Conflicts of Interest: The authors declare that there are no conflict of interest regarding the publication of this paper.

References

1. Li, X.; Li, Z.; Jin, S.; Zhang, J.; Niu, Z.; Liu, J. Contact Properties Research for Linear Sliding Guide Rail with the Fractal Theory. In Proceedings of the ASME 2019 International Mechanical Engineering Congress and Exposition, Calvin L. Rampton Salt Palace Convention Center, Salt Lake City, UT, USA, 11 November 2019.
2. Lu, J.; Pan, B.; Che, T.; Sha, D. Discrete Element Analysis of Friction Performance for Tire-Road Interaction. *Ind. Lubr. Tribol.* **2020**, *72*, 977–983. [CrossRef]
3. Wang, Y.; Gang, L.; Liu, S.; Cui, Y. Coupling Fractal Model for Fretting Wear on Rough Contact Surfaces. *J. Tribol.* **2020**, *143*, 091701. [CrossRef]
4. Hao, Q.; Yin, J.; Liu, Y.; Jin, L.; Zhang, S.; Sha, Z. Time-varying Wear Calculation Method for Fractal Rough Surfaces of Friction Pairs. *Coatings* **2023**, *13*, 270. [CrossRef]
5. Zuo, X.; Zhou, Y.; Ma, C.; Fang, H. Dynamic Identification of Wear State Based on Nonlinear Parameters. *Fractals* **2019**, *27*, 1885–1891. [CrossRef]
6. Xu, C.; Wu, T.; Huo, Y.; Yang, H. In-situ Characterization of Three Dimensional Worn Surface under Sliding-Rolling Contact. *Wear* **2019**, *426–427*, 1781–1787. [CrossRef]
7. Godet, M. The Third-body Approach a Mechanical View of Wear. *Wear* **1984**, *100*, 437–452. [CrossRef]
8. Berthier, Y.; Colombie, C.; Vincent, L.; Godet, M. Fretting Wear Mechanisms and Their Effects on Fretting Fatigue. *J. Tribol. -Trans. Asme* **1988**, *110*, 517–524. [CrossRef]
9. Eriksson, M.; Bergman, F.; Jacobson, S. On the Nature of Tribological Contact in Automotive Brakes. *Wear* **2002**, *252*, 26–36. [CrossRef]
10. Xu, G.-Z.; Liu, J.-J.; Zhou, Z.-R.; Zhon, Z.-R. The Effect of the Third Body on the Fretting Wear Behavior of Coatings. *J. Mater. Eng. Perform.* **2002**, *11*, 288–293. [CrossRef]
11. Cao, M. *Effect of Braking Condition on the Friction and Wear Properties of Brake Pad*; Dalian Jiaotong University: Dalian, China, 2008. (In Chinese)
12. Dolgopolov, K.N.; Lyubimov, D.N.; Ponomarenko, A.G.; Chigarenko, G.G.; Boiko, M.V. The Structure of Lubricating Layers Appearing during Friction in the Presence of Additives of Mineral Friction Modifiers. *J. Frict. Wear* **2009**, *30*, 377–380. [CrossRef]
13. Yang, Y. *Study on the Third Body on the Surface of Brake Disc Material*; Beijing Jiaotong University: Beijing, China, 2012. (In Chinese)
14. Bulnes, R. Mechanochemical Friction of Third-body as an Exergetic Collision. *Tribol. Online* **2011**, *6*, 55–63. [CrossRef]
15. Perumean, D.W. The Force Between Two Sliding Bodies When Observed from a Third Moving Body. *Tribol. Online* **2011**, *6*, 185–188. [CrossRef]
16. Lei, B.; Yi, M.; Xu, H.; Ran, L.; Ge, Y.; Peng, K. Microstructures of the Worn Surface Layer of C/C Composites. *Acta Mater. Compos. Sin.* **2010**, *27*, 64–69.
17. Diomidis, N.; Mischler, S. Third Body Effects on Friction and Wear during Fretting of Steel Contacts. *Tribol. Int.* **2011**, *44*, 1452–1460. [CrossRef]
18. Stoyanov, P.; Romero, P.A.; Järvi, T.T.; Pastewka, L.; Scherge, M.; Stemmer, P.; Fischer, A.; Dienwiebel, M.; Moseler, M. Experimental and Numerical Atomistic Investigation of the Third Body Formation Process in Dry Tungsten/Tungsten-Carbide Tribo Couples. *Tribol. Lett.* **2013**, *50*, 67–80. [CrossRef]
19. Lepesant, P.; Boher, C.; Berthier, Y.; Rézai-Aria, F. A Phenomenological Model of the Third Body Particles Circulation in a High Temperature Contact. *Wear* **2013**, *298–299*, 66–79. [CrossRef]

20. Su, L.; Gao, F.; Han, X.; Chen, J. Effect of Copper Powder Third Body on Tribological Property of Copper-based Friction Materials. *Tribol. Int.* **2015**, *90*, 420–425. [CrossRef]
21. Gao, F.; Miao, J.; Han, X.; Fu, R.; Chen, J. Relationship between Arrangement Patterns and Tribological Properties of Copper-aluminum-graphite Materials. *Ind. Lubr. Tribol.* **2016**, *68*, 170–175. [CrossRef]
22. Zhu, T.; Shipway, P.; Sun, W. The Dependence of Wear Rate on Wear Scar Size in Fretting; The Role of Debris Expulsion from the Contact. *Wear* **2019**, *440–441*, 203081. [CrossRef]
23. Liskiewicz, T.; Kubiak, K.; Mann, D.; Mathia, T. Analysis of Surface Roughness Morphology with TRIZ Methodology in Automotive Electrical Contacts, Design against Third Body Fretting-corrosion. *Tribol. Int.* **2020**, *143*, 106019. [CrossRef]
24. Zhang, P.; Zhang, L.; Wei, D.; Wu, P.; Cao, J.; Shijia, C.; Qu, X. Substance Evolution and Wear Mechanism on Friction Contact Area of Brake Disc for High-speed Railway Trains at High Temperature. *Eng. Fail. Anal.* **2020**, *111*, 104472. [CrossRef]
25. Jayanta, M.; Karabi, D.; Siddhartha, D. An Investigation of Mechanical Property and Sliding Wear Behavior of 400HV Grade Martensitic Steels. *Wear Int. J. Sci. Technol. Frict. Lubr. Wear* **2020**, *458–459*, 203081.
26. Hu, J.; Yuan, F.; Liu, X.; Wei, Y. Effect of Plasticity on Nanoscale Wear of Third-body Particles. *Tribol. Int.* **2021**, *155*, 106739. [CrossRef]
27. Ahmadi, A.; Sadeghi, F. A Novel Three-Dimensional Finite Element Model to Simulate Third Body Effects on Fretting Wear of Hertzian Point Contact in Partial Slip. *J. Tribol.* **2021**, *143*, 4048386. [CrossRef]
28. Shpenev, A.G.; Muravyeva, T.I.; Shkalei, I.V.; Bukovskiy, P.O. Influence of the Surface Film (Third Body) on the Friction and Wear Process of Carbon-Fiber Composites. *J. Surf. Investig.* **2022**, *16*, 397–401. [CrossRef]
29. Li, Y.; Schreiber, P.; Schneider, J.; Greiner, C. Tribological Mechanisms of Slurry Abrasive Wear. *Friction* **2023**, *11*, 1079–1093. [CrossRef]
30. Brink, T.; Milanese, E.; Molinari, J.F. Effect of Wear Particles and Roughness on Nanoscale Friction. *Phys. Rev. Mater.* **2022**, *6*, 136–142. [CrossRef]
31. Wang, J. *Research on the Evolution Behavior of Third-Body Layer on the Surface of SiCp/A356 Composites under Service Environment*; Beijing Jiaotong University: Beijing, China, 2018. (In Chinese)